RESEARCH ARTICLE

RSP Science Hub

International Research Journal on Advanced Science Hub
2582-4376
www.rspsciencehub.com
Vol. 08, Issue 05 May

Check for updates

http://dx.doi.org/10.47392/IRJASH.2026.025

ASeO-CNN: Active Search Optimization-enabled Convolutional Neural Network for Channel estimation on Fifth Generation wireless channels

Sarika Sudhakar Apshankar[1], Dr. Chandani Sharma[2]
[1]PhD Scholar-, Shri Vyakateshwara University, Gajraula, Uttar Pradesh
[2]PhD-Guide, Shri Vyakateshwara University, Gajraula, Uttar Pradesh
Emails: *sareeka.anr07@gmail.com[1], chandani19nov@gmail.com[2]*

Article history
Received: 25 April 2026
Accepted: 24 May 2026
Published: 02 July 2026

Keywords:
Deep learning, Wireless communication, channel estimation, Pilot signals, Spectral efficiency.

Abstract
Channel estimation remains a crucial requirement to ensure efficient spectrum usage, enhance the network performance, and reliable data transmission in fifth-generation wireless communication systems. The prevailing channel estimation methods struggle with reduced latency, pilot overhead, and higher computational complexity in dynamic wireless communication environments. Henceforth, the research proposes an Active Search Optimization-enabled Convolutional Neural Network(ASeO-CNN) for channel estimation. Through leveraging the intrinsic complex feature extraction characteristics, the model acquires the complex channel features from the orthogonal frequency division multiplexing signals. Meanwhile, the Active Search Optimization(ASeO) employed optimizes the model hyperparameters and helps in enhancing the convergence speed and channel estimation accuracy. Furthermore, the Quadrature Amplitude Modulation(QAM) scheme helps in reliable data transmission through evaluating the complex channel characteristics significantly. Experimental findings with a 20dB Signal to Noise Ratio demonstrate the improved channel estimation performance by achieving 5.32 x 10-5 Bit Error Rate, 0.97 correlation, 0.13 Mean Absolute Error, 0.040 Mean Squared Error, and 0.933 R-Squared metrics.

1. Introduction

The exploding demand for successful data transmission increases the requirement for next-generation networks, provided with thousands of antennas, along with the utilization of terahertz frequency bands [9]. The Channel estimation concept development helps enhance the wireless communication system performance[10]. In general, the signal received at the receiver end exhibits distortions due to the varying characteristics. Hence, as a means of recovering the transmitted signal, channel estimation is performed and compensated at the receiver end[11,12]. Channel estimation is defined to be the accurate acquisition of the Channel State Information(CSI). The most familiar method adopted for channel estimation is the channel coefficient estimation based on the pilot symbol method[13]. Depending on the pilot symbol utilization, the channel estimation is categorized into pilot-aided channel estimation, semi-blind channel estimation, and blind channel estimation[14]. Both the blind and semi-blind channel estimation are applicable for Wide-Sense Stationary(WSS) channels, while the pilot-aided models are more suitable for doubly

selective channels[15].

Frequency-domain estimation and time-domain estimation are the two diverse methods used for channel estimation. In the frequency-domain-based channel estimation, the Channel Frequency Response(CFR) of the pilot symbol is determined and interpolated with the CFR of the transmitted data symbol[16,17]. While the Channel Impulse Response(CIR) is determined in the time-domain-based estimation method, which supports active elimination of the Inter Carrier Interference(ICI)[18,19]. Linear Minimum Mean Square Error(LMMSE) and the Least Squares(LS) are the most commonly used frequency-domain channel estimation methods. Yet, performing channel estimation based on the assumption that the CIR remains continuous throughout the channels made its unfit for usage in high-speed environments[20,21]. Even though the time-domain estimation method estimated the CIR reliably, the requirement for too many estimation parameters increased the estimation complexity and limited its wider usage[22,23]. Hence, estimation performance, Machine Learning (ML) models are designed to enhance channel performance through performing fault identification, channel coding, power optimization, dynamic spectrum sharing, and symbol detection[24,25].

Recently, Deep Learning (DL)-based Artificial Intelligence (AI) models have been used in channel estimation, as they aid in the proper estimation of the CSI via the elimination of the dimensionality curse issues [26]. The neural networks involved in the DL models enable better mapping of the pilot signals to the channel estimates using their supervised learning characteristics. Yet, the measurement-specific and reduced generalizability of these supervised DL models limited their significance in channel estimation [29]. In essence, the deep generative models, including the Diffusion Models(DM), Gaussian Mixture models, Variational AutoEncoders, and Generative Adversarial Networks(GANs), accurately synthesized the high-dimensional data using their potential in acquiring the highly complex relationships[30,31]. Furthermore, the score-based Generative(SGMs) were also designed to achieve better estimation accuracy[32]. However, the presence of numerous inference steps in these models failed to achieve better latency and increased the substantial computational burden[33]. Furthermore, the resource scarcity and the higher decoding errors limited the effectiveness of the data-aided channel estimation models [34, 35].

The research develops a DL-based channel estimation method named ASeO-CNN with fine-tuned hyperparameters to mitigate the uncertainties in performing channel estimation. The incorporation of the reliable pilot symbols reduces the erroneous detection impacts on channel estimation accuracy. Moreover, the QAM scheme utilization reinforces the scalability of the AseO-CNN to higher-order modulation with lower latency. Some of the significant contributions are listed further.

- ***Active Search Optimization:*** The ASeO algorithm integrates the anti-prediction and foraging behaviors of sparrow search in attaining the global best position with the three distinct exploitation characteristics of the squirrel search to fine-tune the ASeO-CNN's hyperparameters. The adjustment mechanism promotes a wider search to find the best region by eliminating the random errors.
- ***Active Search Optimization-enabled Convolutional Neural Network:*** The AseO-CNN accurately estimates the channel coefficients of the wireless networks through capturing the intricate spatial correlation. Further, the QAM scheme and the pilot symbols provided better estimation performance under high data rates with lower latency. Collectively, the AseO-CNN, with its fine-tuned hyperparameters, improves the generalization ability with a reduction in overfitting risks when trained with diverse training percentages.

2. Literature Review

The following are some of the recent works on channel estimation, listed with their downsides as follows.

Hamidreza Hashempoor and Wan Choi[1]introduced a Deep Neural Network (DNN) model to perform channel estimation. The denoising block incorporated within this approach enabled accurate extraction of noiseless embeddings to correctly distinguish the detected data using the correctness classifier. In addition, it also ensured reliable channel estimation performance through direct data detection. On the other hand, the reduced scalability and generalizability posed a crucial

challenge in channel estimation with an increase in computational complexity. Al-Imran *et al.*[2] presented a Deep Attentional Residual U-Net(ARU-Net) for channel estimation in a massive communication system. The functions of both the attention and the residual layers were combined in the UNet to accurately retrieve the channel coefficient matrix through mitigating the noise effects. Yet, the complex mathematical calculations involved in estimating the channel states made the process hugely challenging due to the varying atmospheric turbulence.

Xingyu Zhou *et al.*[3] developed a Diffusion Model(DM)-based posterior inference approach to perform channel estimation. The Stein's Unbiased Risk Estimator(SURE) integrated within the DM enabled its learning ability to handle noisy data with better scalability. The application of the Monte-Carlo approximation reduced the computational complexity. Conversely, its robustness was highly affected due to the phase ambiguities. Apitchaya Siriwanitpong *et al.*[4] evinced a one-dimensional CNN(1D CNN) with scattered pilot symbols to perform channel estimation. The deployment of the scattered pilot symbols within the restricted 1D-CNN increased the transmission efficiency and adaptability to incorporate within the reduced input. However, its inability to handle multi-dimensional complex data reduced its performance in channel estimation.

Yiquan Gao *et al.*[5] modeled an Enhanced DM(EDM) model to perform joint channel estimation. The step-size network(stepnet) developed for controlling the update steps involved in joint channel estimations eliminated the layer-wise backpropagation complexity and reduced the computational overhead. On the contrary, higher error propagation challenges posed a significant risk in data transmission. Peicong Zheng *et al.*[6] propounded CNN-based Convolutional Dictionary Learning(CNN-CDL) to perform channel estimation. The Proximal Gradient Descent(PGD) and the cross-layer feature integration incorporated in the CNN-CDL reduced the complexity in capturing the hybrid-field channel structure and gradient computation. Yet, the higher pilot overhead reduced its significance in channel estimation.

Zhongnian Li *et al.*[7] exaggerated a U-shaped Mamba model named CP-Mamba for channel estimation. Apparently, the Mambal model and the U-shaped convolutional networks integrated in the CP-Mamba reduced the channel estimation errors through capturing long-range dependences and local spatial features. However, the delicate multi-stage and complex network tuning requirements of the U-shaped network increased the convergence issues. Xinyu Tian and Qinghe Zheng[8] developed a hybrid DL model with the Stochastic Gradient Descent(SGD) mechanism to perform channel estimation. Integrating the spatial analysis characteristics of the CNN with the temporal feature handling characteristics of the LSTM enabled better generalizability in handling complex channel conditions. Conversely, the reduced adaptability to the varying environmental conditions increased the computational demand and made the decision-making process hugely difficult.

2.1. Challenges

Certain key challenges in channel estimation are provided below.

- ❖ The presence of a large number of network parameters and the inference steps in the DM-based models increased the phase ambiguities in data transmission[3].
- ❖ The presence of a huge number of users in the network reduced the data transmission rate, increased the computational complexities, and scalability challenges[1].
- ❖ The large number of reconfigurable intelligent surfaces present in the CNN-CDL increased the pilot overhead in channel estimation[6].
- ❖ The delicate multi-stage and complex network tuning requirements of the U-shaped network increased the convergence issues in CP-Mamba-based channel estimation models[7].

2.2. Problem Formulation

Accurate estimation of the channel state details helps in enhancing the data transmission reliability with reduced signal distortions and interferences. Despite the remarkable achievements made using the DL models in channel estimation, the requirement for huge amounts of data[1] and computing resources[8] for training made channel estimation crucially challenging in resource-constrained systems. Further, structural complexity constraints of the DL model increased the interpretability[5], pilot overhead, and convergence problems[7]. Henceforth, the research designs AeSO-CNN to analyze the channel characteristics to initiate reliable data transmission.

Consider a wireless communication system with

N_m number of transmitting antennas and N_n number of receiving antennas in the 5G communication environment. Let $X(t)$ be the data transmitted in the wireless communication system in binary form with t time slots using the Quadrature Amplitude Modulation(QAM) scheme. The vector representation of the symbols present in $X(t)$ is given in (1).

$$X(t)=\left[X_1(t),X_2(t),X_3(t),...,X_N(t)\right] \quad (1)$$

Here N indicates the maximum number of modulation symbols. These modulated data transmitted from N_m transmitting antenna, denoted as $X_i(t)$ are further split into N_m vectors as given in (2).

$$X_i(t)=\left[X_{i+N_m}(t),X_{i+2N_m}(t),...\right];i=\{1,2,3,...,N_m\} \quad (2)$$

The QAM modulated data, thus obtained, exhibits Serial to Parallel(S/P) conversion to generate multiple parallel streams of data. Thereby, eliminating the ISI and enables the accurate insertion of the pilot signals. Apparently, one column of the data symbol represents a single OFDM symbol, whereas multiple columns of the OFDM symbol form the OFDM grid. Typically, each row of the data symbol is termed a subcarrier. Eventually, the presence of "N"data symbols within a single OFDM symbol ensures "N"the number of subcarriers present in it.

Herein, pilot symbol insertion signifies the phenomenon of embedding the known data in the OFDM symbol. Following the pilot symbol insertion, S/P conversion takes place along the data in each layer. Now, the data in the frequency domain is transformed back to the time domain via the application of the Inverse Fast Fourier Transform (IFFT). Then, Parallel to Serial(P/S) conversion takes place, after the insertion of the Cyclic Prefix(CP) into the signal to be transmitted through the channel from the transmitter to provide better protection against ISI. The signal thus received at the receiver modeled as $R(k)$ is mathematically defined in (3).

$$R(k)=\hbar(k)\delta(k)+\eta(k) \quad (3)$$

Here $\hbar(k)$ represents the channel matrix of the k^{th} symbol whose elements signify the channel coefficients, $\delta(k)$ unveils the pilot symbol matrix, $\eta(k)$ indicates the noise channel matrix. Then $\hbar(k)$ is determined as given in (4), using the details provided by $R(k)$.

$$\hbar(k)=\Im g \quad (4)$$

Where g signifies the channel vector in the time domain, $\Im$ models the Fast Fourier Transform Matrix. The formula used for channel estimation using the LS estimator$\left(\bar{\square}_{LS}\right)$ with no details regarding the channel statistics, is given in (5).

$$\bar{\square}_{LS}=\left[X_i(t)\right]^{-1}R(k) \quad (5)$$

$R(k)$ thus received at the receiver exhibits space-time demodulation and space-time equalization to ensure reliable processing of the signals received at different antennas. Apparently, the time-to-frequency domain transformation of the received OFDM symbol takes place via the FFT application after S/P conversion and CP removal. The pilot symbols are extracted, and the data streams at different antennas are then converted into a single signal stream through P/S conversion. Substantially, channel estimation takes place using the ASeO-CNN in the 5G channel using $R(k)$ and the known details or the extracted pilots. Now, the output obtained is the subcarrier symbol comprising both the data stream and the pilot symbols. Next, signal demodulation takes place to generate the baseband signal, with the restored crucial details sent by the transmitter. The significance of the ASeO-CNN-based channel estimator is analyzed in light of the minimization of the Mean Absolute Error(MAE) (X_{mae}) and is expressed in (6).

$$X_{mae}=\frac{1}{N}\sum_{i=1}^{N}\left|R_i-\hat{R}_i\right| \quad (6)$$

Here $\hat{R}_i$ denotes the prediction result of the ASeO-CNN, N represents the total number of data, R_i stands for the actual channel estimation output.

Thereby, the research ensures that ASeO-CNN supports accurate capturing of the channel details to enable reliable data transmission under diverse wireless communication criteria. The complex channel details capturing ability of the convolutional filters reduced the computational burden in the high-dimensional space. Specifically, the development of the ASeO algorithm to fine-tune

the ASeO-CNN's hyperparameters enabled end-to-end optimization with reduced convergence issues and improved generalizability on unseen data.

3. System Model for channel estimation in 5G wireless networks

The Orthogonal Frequency Division Multiplexing (OFDM) system used for data or symbol transmission comprises a large number of subcarriers for each data or symbol. Two crucial components, including the transmitter and the receiver, are present in the OFDM to support active user data transmission via the multipath fading channel. Apparently, the input data gets modulated on the transmitter side using any of the modulation techniques, including the QAM, Binary Phase Shift Keying(BPSK), and Quadrature Phase Shift Keying(QPSK), to track the variation in channel characteristics. The pilot insertion helps in enhancing the channel estimation accuracy. In particular, the cyclic prefix and the pilot symbols are added to enhance the protection against ISI and to perform channel estimation. The signal received at the receiver is usually in the time domain and is accompanied by the noise component, specifically the Additive White Gaussian Noise(AWGN). Performing channel estimation using the DL model generates the equalized signal by compensating for the channel effects. Further demodulation ensures the regeneration of the transmitted data. Hence, channel estimation is practically used for maximizing the data rates, direct data transmission, and multipath distortion removal. The system model for the channel estimation is given in Figure 1.

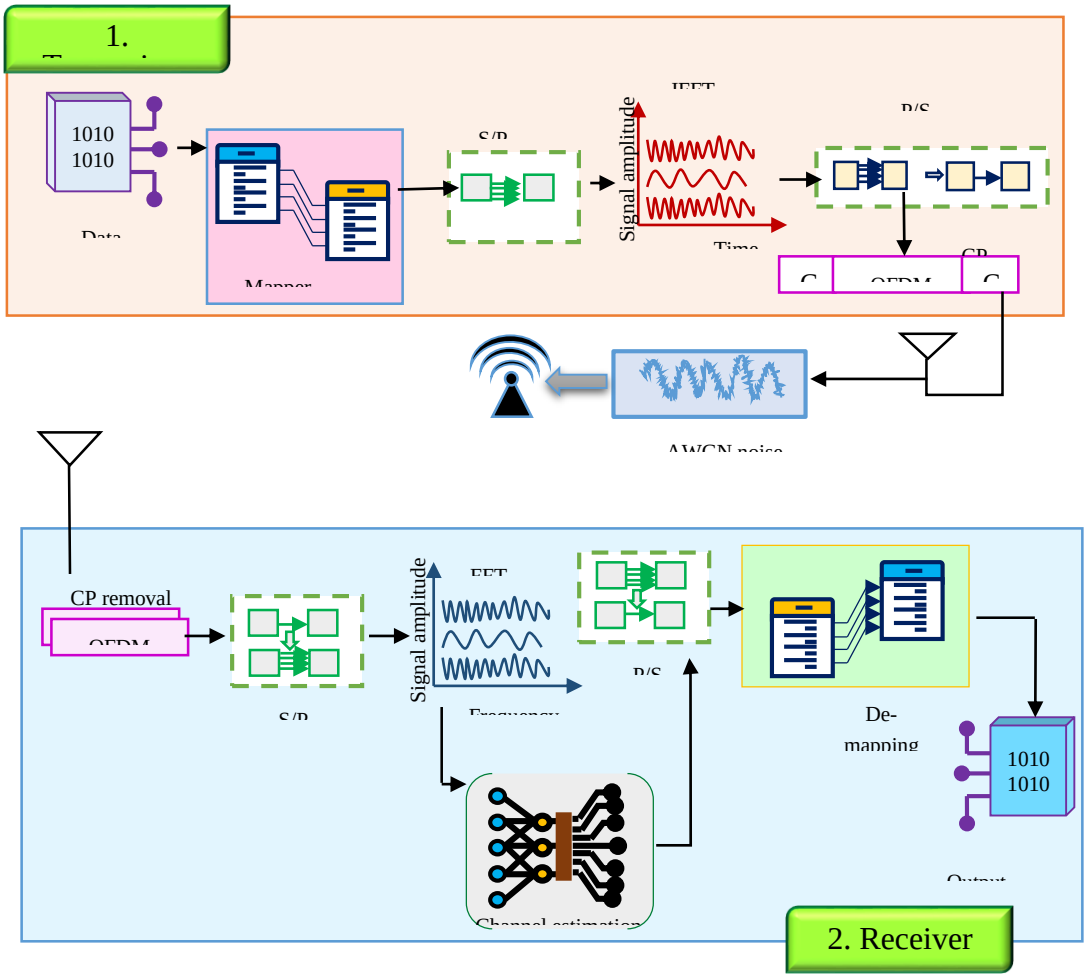

Figure 1 System Model for Channel Estimation in Wireless Networks

4. Proposed Active Search Optimization-enabled Convolutional Neural Network for channel estimation in 5G wireless networks

The research proposes ASeO-CNN for channel estimation in 5G wireless networks. The research begins by transmitting the data in binary form. Initially, the binary data streams exhibit QAM-based data modulation to ensure reliable

transmission with maximal spectral efficiency through encoding the binary data in bits to a single transmitted symbol. The QAM-modulated data is then intermixed with pilot symbols to measure the CFR and to ensure channel equalization. The signal thus obtained then exhibits S/P conversion to generate high-speed parallel sub-streams. Now, the IFFT operation is applied to the parallel sub-stream data symbols to generate the time-domain data symbols. After that, CP insertion takes place to ensure protection against ISI, followed by which is the signal transmission through the channel with AWGN in a serial manner. The signal thus received at the receiver exhibits the reverse process that takes place during the signal transmission to output the final recovered data. Eventually, after extracting the pilot symbols at the receiver side, the channel estimation takes place using the ASEO-CNN with fine-tuned hyperparameters. The diagrammatic modelling of channel estimation using ASeO-CNN is provided in Figure 2.

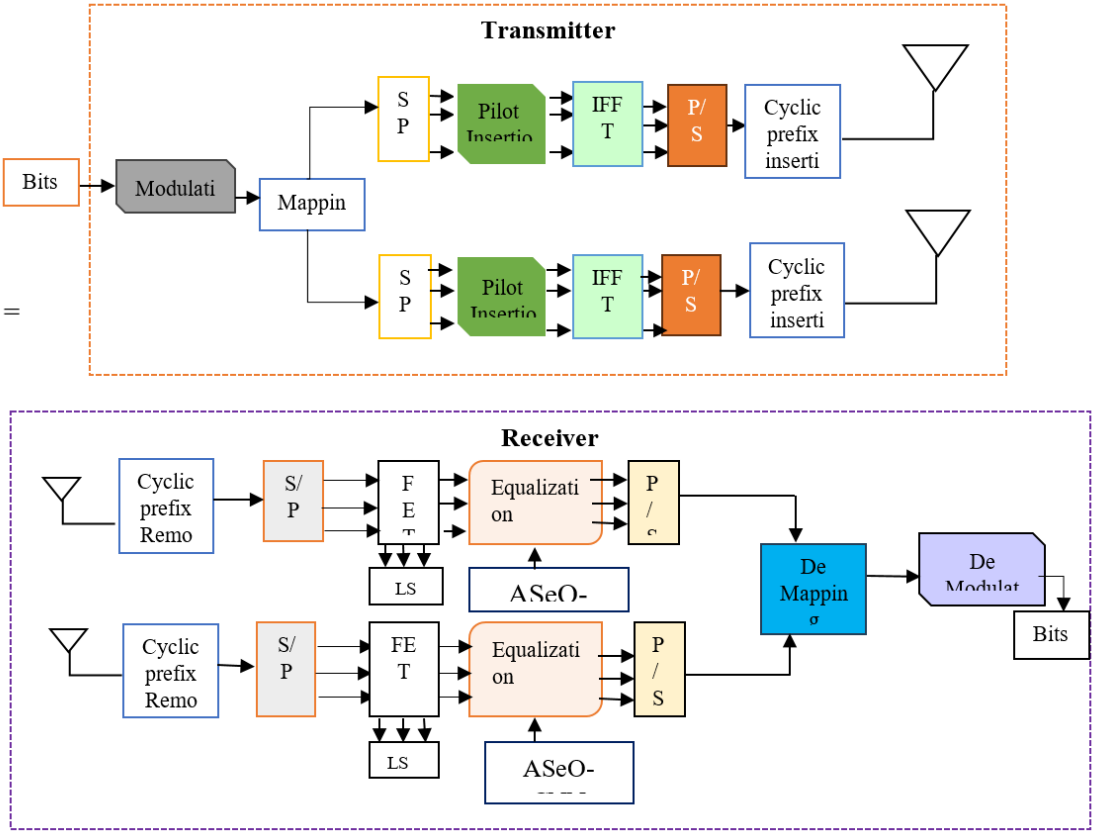

Figure 2 Diagrammatic modelling of the ASeO-CNN

4.1. Input Bits

To perform ASeO-CNN-based channel estimation, let us consider an OFDM system in an isotropic scattering environment with MIMO characteristics. Herein, the transmitter used for transmitting $X(t)$ to the receiver (Rr) is denoted as Tr. Apparently, the antenna arrays present in Tr and Rr within the MIMO-OFDM system with sufficient spacing are modelled N_m and N_n.

4.2. Data transmission in the Transmitter

The transmitter initiates the data transmission through the MIMO channel with 5G channel profiles, by firstly converting $X(t)$ into encoded data, which is further mapped to the relevant symbol set. The symbol sequence is further analyzed using the space-time coding mechanism to enhance the fault tolerance and anti-inference characteristics of the MIMO-OFDM system. These binary data further exhibit QAM-based modulation to enhance the data throughput by modeling the binary data into symbol sequences along the amplitude and phase values. In essence, the ability of the QAM to allow reliable transmission of the signals with multilevel

amplitude modulations using the same carrier frequency helps in effective preservation of the spectrum bandwidth. The modulated symbol sequence used for transmission is modeled as $X_i(t)$.

Specifically, $X_i(t)$ thus obtained is then assigned to one of the "E" subcarriers. Eventually, these symbol sequences are intermixed with the pilot symbols to ensure channel equalization. Substantially, these pilot symbols are assigned to the subcarriers whose positions are predetermined, while the rest of the subcarriers remain dedicated to the transmission symbol sequences. In case of allocating $X_i(t)$ to a^{th} subcarrier of the f^{th} transmitting antenna with t^{th} index, then $X_i(t)$ is represented as $X_f(a,t)$. Specifically, the vector representation for $X_i(t)$ in t^{th} time is given as $X_f(t)$. The formula for $X_f(t)$ is given in (7).

$$X_f(t) = \left[X_f(1,t), ..., X_f(E,t) \right] \tag{7}$$

These QAM-modulated symbol vectors are then converted into parallel substreams to reduce the symbol rate and enhance the spectral efficiency by exhibiting S/P conversion. Each of the parallel substreams then undergoes an IFFT as given in (8) to transform $X_f(t)$ in the frequency domain to the time domain.

$$\hat{X}_f(t) = IFFT\left[X_f(t) \right] \tag{8}$$

Here $\hat{X}_f(t)$ corresponds to the time-domain signal. After that, the CP is inserted into $\hat{X}_f(t)$ to mitigate the discrepancies in reliable signal transmission, such as ICI and ISI. The signal thus obtained after CP insertion modeled as $\hat{x}_f(t)$ is then transmitted serially via the Multipath OFDM channel with AWGN. The addition of the AWGN in signal transmission helps in optimizing the receiver performance using its zero mean and variance with circular Gaussian characteristics. In addition, the AWGN inclusion supports an accurate evaluation of the communication system performance, through accounting the genuine noise channel characteristics.

Herein, the channel impulse response from the f^{th} transmitting antenna $\left(f \in \{1, ..., N_m\} \right)$ is defined to be a Linear Time Variant (LTV) channel vector modeled as $\vartheta_{f,l}(\varsigma_z, t)$ with the l^{th} receiving antenna $\left(l \in \{1, ..., N_n\} \right)$. The formula for $\vartheta_{f,l}(\varsigma_z, t)$ is given in (9).

$$\vartheta_{f,l}(\varsigma_z, t) = \vartheta_z e^{j2\pi d_{shift}, z(t-\varsigma_z)} e^{-j2\pi \bar{f}_c \varsigma_z} \tag{9}$$

Where ϑ_z stands for the amplitude of the z^{th} path, ς_z represents the z^{th} path's delay, d_{shift}, z interprets the Doppler shift, $\bar{f}_c$ indicates the carrier frequency. From these characteristics, it is evident that the multipath OFDM channel accounts for both the time-selective and frequency-selective fading through acquiring the Doppler shift and multi-path propagation effects.

4.3. 4.2 Signal reception at the receiver

The signal received at the l^{th} receiving antenna on the receiver side in the time domain is represented as $y_l(t)$ in (10).

$$y_l(t) = \sum_{f=1}^{N_m} \vartheta_{f,l}(t) * \hat{x}_f(t) + \varpi_l(t) \tag{10}$$

Here $*$ represents the convolution operation, $\varpi_l(t)$ stands for the AWGN. Eventually, the mathematical formulation for the channel vector from f^{th} transmitting antenna to l^{th} receiving antenna with time index (t) is given as $\vartheta_{f,l}(t)$ in (11).

$$\vartheta_{f,l}(t) = \left[\vartheta_{f,l}(\varsigma_1, t), ..., \vartheta_{f,l}(\varsigma_M, t) \right] \tag{11}$$

Where ς_M signifies the M^{th} path delay. The frequency domain representation of $\vartheta_{f,l}(t)$ is indicated as $\tilde{\vartheta}_l(t)$ and is formulated in (12).

$$\tilde{\vartheta}_l(t) = \sum_{f=1}^{m} \tilde{\vartheta}_{f,l}(t) \square X_f(t) + \tilde{\varpi}_l(t) \tag{12}$$

Here $\square$ unveils the pointwise product, $\tilde{\vartheta}_{f,l}(t)$ unveils the channel vector of length E, which remains equivalent to $\zeta\left\{ \vartheta_{f,l}(t) \right\}$, $\tilde{\varpi}_l(t)$ stands for the noise vector with the size of E. The formula for $\tilde{\vartheta}_{f,l}(t)$ is given in (13).

$$\tilde{\vartheta}_{f,l}(t)=\left[\tilde{\vartheta}_{f,l}(1,t),...,\tilde{\vartheta}_{f,l}(E,t)\right] \quad (13)$$

Apparently, $y_l(t)$ undergoes the reverse steps, including the S/P conversion, Removal of CP, FFT application, and pilot extraction, followed by the ASeO-CNN-based channel estimation, and demodulation to recover the original data. Accordingly, the channel estimation begins by extracting the pilot symbols from $y_l(t)$. The pilot symbol thus extracted from $y_l(t)$ received at the l^{th} receiving antenna is given as $\tilde{\vartheta}_l^{pilot}(t)$ in (14).

$$\tilde{\vartheta}_l^{pilot}(t)=\sum_{f=1}^{N_m}\tilde{\vartheta}_{f,l}(t)\, X_f^{pilot}(t)+\tilde{\varpi}_l^{pilot}(t) \quad (14)$$

Where $X_f^{pilot}(t)$ models the known pilot symbol, with a time index (t) at the f^{th} transmitting antenna, $\tilde{\varpi}_l^{pilot}(t)$ corresponds to the noise vector at the l^{th} receiving antenna with a time index (t). Particularly, to determine the CFR, the research uses the LS method at the receiver end is formulated as $\tilde{\vartheta}_{f,l}^{ls}(t)$ in (15).

$$\tilde{\vartheta}_{f,l}^{ls}(t)=\frac{\tilde{\vartheta}_l^{pilot}(t)}{X_f^{pilot}(t)} \quad (15)$$

The CFR, thus estimated using the LS, helps in equalizing, $y_l(t)$ followed by demodulation to generate the actual data.

4.4. Proposed Active Search Optimization-based Convolutional Neural Network channel estimation model

The research presents the ASeO-CNN model for channel estimation in the 5G wireless network system. Presently, several channel estimation methods have been developed; however, the relatively lower spectrum utilization and anti-interference characteristics [2], reduced data transmission rate [1], phase ambiguities [3], pilot overhead [6], and error propagation issues [5] have reduced their significance in estimating the channel characteristics to enable reliable data transmission. The ASeO-CNN model addresses these obstacles in channel estimation through estimating the channel frequency response over all the subcarriers. Specifically, the intrinsic spatial correlation acquisition nature of the CNN eliminates the risk of overfitting and improves the performance on the unseen data. The ASeO-CNN model is illustrated in Figure 3.

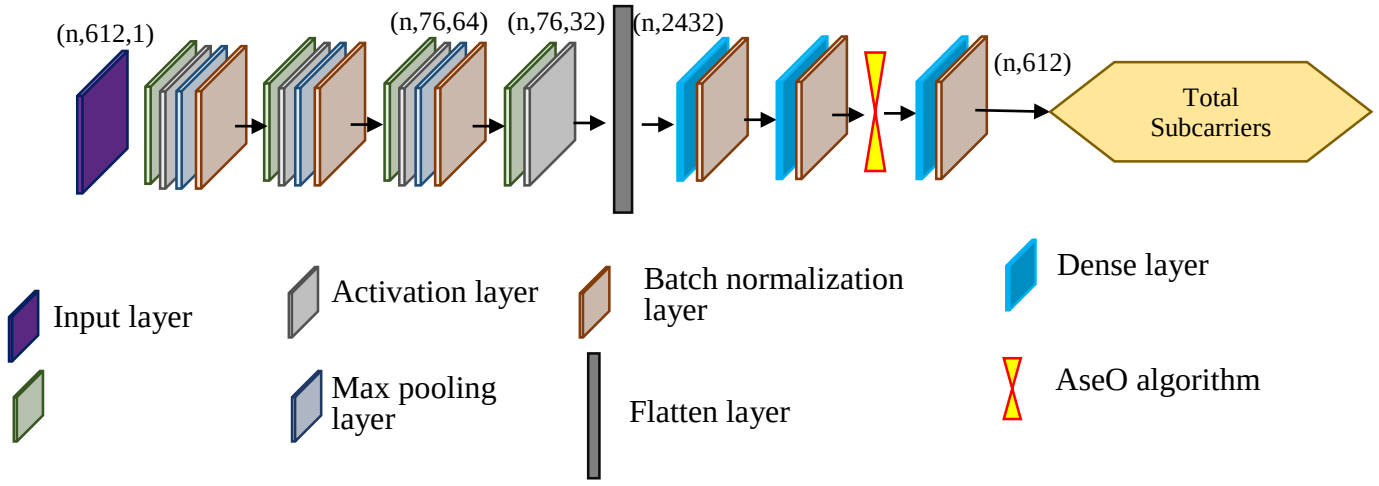

Figure 3 Illustration of the ASeO-CNN model

The AseO-CNN works explicitly for each of the OFDM symbols by getting its input in a single real-valued form of size $(n,612,1)$, denoted as A_{in}. Herein, n represents the total number of samples representing the OFDM grid with added pilot symbols. A_{in} initially enters the convolution layer, which is suitable for analyzing the time series signal data. Accordingly, A_{in} exhibits a 1D convolution operation using the convolution kernel (κ) as given in (16) to leverage the essential features (f_{conv}).

$$f_{conv}=\wp\left[A_{in}*\hat{w}\right]+\hat{B} \quad (16)$$

Where $\wp$ indicates the activation function, $\hat{w}, \hat{B}$ stands for the weight values and Bias values of the AseO-CNN model. f_{conv} is further analyzed in the activation layer, which is followed by dimensionality reduction in the subsequent max-pooling layer. These dimension-reduced features are further normalized in the batch normalization layer to generate the normalized features of dimension $(n, 76.64)$ as output. Thereby ensuring efficient training with reduced vanishing gradient issues. These normalized features further propagate through the subsequent 1D convolution layer and the activation layer to generate informative features of dimension $(n, 76, 32)$. The subsequent flatten layer flattens the incoming informative features into a single-dimensional feature vector of dimension $(n, 2432)$ for easy analysis in the preceding dense layer. Conceptually, the AseO algorithm is deployed next to the dense layer to accelerate convergence through fine-tuning the hyperparameters. The single-dimensional feature vectors flow into two successive dense layers, which are provided with layers of interconnected neurons for intense analysis. Particularly, the final dense layer acts as a classification layer and provides the total number of subcarriers along the frequency axis as output (A_{out}) with dimension $(n, 612)$ upon the application of the softmax activation function. Specifically, the research uses the MAE loss function formulated as X_{mae} in (6) to determine the ability of the AseO-CNN to predict the output. Eventually, updating the AseO-CNN's weight and bias parameters using the AseO-CNN minimizes the loss value and enhances the channel estimation significance.

4.4.1. Proposed Active Search Optimization Algorithm

The ASeO algorithm helps in preventing the ASeO-CNN from getting stuck in a local optimum or convergence issues through fine-tuning its hyperparameters. Even though an enormous number of algorithms are designed to fine-tune the model hyperparameters, the prevalence of stagnation issues, convergence risks, and higher computational burden reduced their fine-tuning significance. Apparently, the ASeO algorithm overcomes these uncertainties in hyperparameter fine-tuning through integrating the exploitation, intermediate improvement, and exploration characteristics of the standard squirrel search[27] within the sparrow search[28] algorithms. Conceptually, the ASeO algorithm is induced in the eighteenth layer of the ASeO-CNN to support optimal convergence and is detailed as follows.

Solution Initialization: The ASeO algorithm starts by initializing n the number of solution modelled as $S \in \{\hat{w}, \hat{B}\}$ in the search space of dimension $\hat{d}$. Here, $\{\hat{w}, \hat{B}\}$ represents the weight and bias parameters of the AseO-CNN. The formulation for solution initialization is given in (17).

$$S = \begin{bmatrix} S_{1,1} & . & . & S_{1,j} & . & S_{1,\hat{d}} \\ . & . & . & . & . & . \\ . & . & . & . & . & . \\ S_{i,1} & . & . & S_{i,j} & . & S_{i,\hat{d}} \\ . & . & . & . & . & . \\ S_{n,1} & . & . & S_{n,1} & . & S_{n,\hat{d}} \end{bmatrix} = \begin{bmatrix} S_1 \\ . \\ . \\ S_i \\ . \\ S_n \end{bmatrix}$$

The position of the i^{th} solution after initialization is defined as S_i in (18).

$$S_i = S_v + \xi(S_u - S_v) \quad (18)$$

Here S_v, S_u represents the lower and upper bounds, ξ interprets the random number with a uniform distribution ranging between $[0,1]$.

Fitness Evaluation: After successfully initializing S_i in the search space, the fitness of each solution S is determined to depict the quality of the optimal S determined in the search space. Apparently, the solution with minimal Mean Squared Error(MSE) is considered to be the optimal solution. The formula for fitness evaluation is given in (19) as $F(S_i)$.

$$F(S_i) = \min(MSE(S_i)) \quad (19)$$

Solution Allocations: Followed by the fitness evaluation is the solution allocation phase, which involves the "Active Analysis Phase" and "Active Pursuit Phase". Particularly, the solution with the initial best fitness exhibits the "Active Analysis Phase", while the solution with the remaining or the second half fitness undergoes the "Active Pursuit Phase". Based on which the solutions are sorted as given in (20),

$$S_{soln\,set} = [S_1^*, ..., S_i^*, ..., S_n^*] \quad (20)$$

Here n^* indicates the total number of solutions after sorting based on the fitness values. Specifically, for S_i^* to enter the "Active Analysis Phase" and "Active Pursuit Phase", the following two assumptions are made.

(i) Assume: $i = 1 to \frac{n^*}{2}$, S_i^* is in "Active Analysis Phase."

(ii) Assume: $i = \frac{n^*}{2} to n^*$, S_i^* is in "Active Pursuit Phase."

From the assumptions, it is familiar that the solution with the initial best fitness values exhibits the "Active Analysis Phase", while the remaining half exhibits the "Active Pursuit Phase". A detailed explanation for each of these phases is given below.

Phase 1: *For* $i = 1 to \frac{n^*}{2}$ *: Active Analysis Phase*

The solution (S_i) enters the Active analysis phase if it possesses the initial fitness value as $i = 1 to \frac{n^*}{2}$. Accordingly, the position of the solution exhibiting the Active analysis phase gets updated as S_i^{T+1} and is given in (21).

$$S_i^{T+1} = \begin{cases} S_i^t e^{-\frac{i}{\beta T_{\max}}}, & if\ \gamma < \zeta \\ S_i^T + \square\ G\left(S_{best} - S_i^T\right), & elsewhere \end{cases} \tag{21}$$

Where β indicates the uniform random number given as $\beta \in (0,1)$, $\square$ unveils the random number belonging to the normal distribution, G signifies the direction influence factor, $T, T_{\max}$ denotes the present, and the maximum iterations, γ represents the alertness factor, and is defined as $\gamma \in (0,1)$, ζ corresponds to the crucial control parameter, and is given as $\zeta \in (0.5,1)$, S_{best} defines the globally best solution thus obtained.

Apparently, the solutions exhibiting this phase are considered to be the solution with better fitness factors and positional updation characteristics. Eventually, the two dual factors, namely the γ and ζ present in (21), enable the solution to adjust its position differently. Moreover, in this Phase 1, it is assumed that the solution might continue to make an extensive search in the search region with no dependence on the environmental factors, that acts as an obstacle to making the movement.

In case the environmental factors act as an obstacle and divert the movement of the solution, the solution evolves with additional upgradation factors. Thereby, the solution tries to reduce the difference between the current position and the position of the globally best or the historically best solution. These phenomena thus result in positional improvement with the influential term. Occasionally, the randomness creates an equilibrium between searching for the best solution and the solution that is assumed to be the best.

Phase 2: *For* $i = \frac{n^*}{2} to n^*$ *: ActivePursuit Phase*

The solution (S_i) enters the Active Pursuit phase if it possesses the initial fitness value as $i = \frac{n^*}{2} to n^*$. Accordingly, the position of the solution exhibiting the Active Pursuit phase gets updated as given in (22).

$$S_i^{T+1} = \begin{cases} S_i^t + \Gamma G e^{\frac{S_{best} - S_i}{i^2}}, & if\ \beta_j > \gamma(0,1) \\ S_p - \left|S_i^t - S_p\right| H^+ \ell, & elsewhere \end{cases} \tag{22}$$

Where Γ define the stepsize control factor, S_p unveils the personal best solution, H^+ represents the pseudo-inverse factor, β_j denotes the conditional adjustment factor with its range given as $\{0,2\}$. In this phase, the solution requires numerous updates to make it a leading solution in the search space. To do so, the ASeO algorithm makes use of "Γ" along with an exponential difference between the global and current positions. The introduction of these factors enables the solution to adjust its movement towards the best regions in the search space. Apparently, performing solution updation based on random conditions increases the diversity to determine the optimal solution. These increases in diversity are mainly due to the involvement based on the personal best difference, which results in increased learning via its historical best places. In addition, this adjustment or the shift assumption existing between S_{best} and S_p initiates the solution to

make a wider search before finding out the best region. The flowchart for the ASeO algorithm is provided in Figure 4.

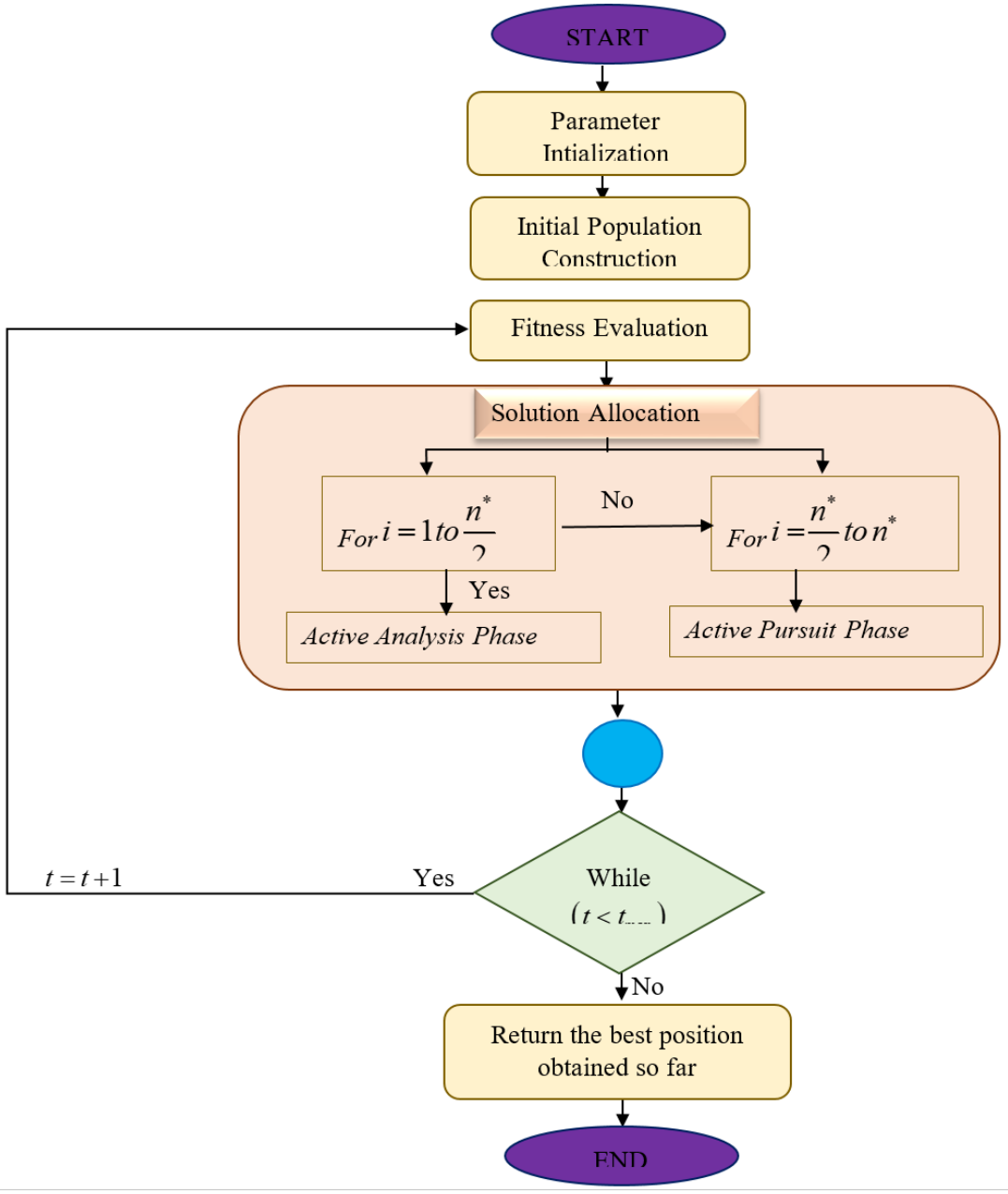

Figure 4 Flowchart for the ASeO algorithm

5. Results and Discussion

The AseO-CNN's performance on Channel estimation in 5G communication networks is explained in this section. Herein, the analysis is made based on the 40% training and 60% testing data splitting strategy. The analysis process is discussed further.

5.1. Experimental Setup

The AseO-CNN is implemented in Python 3.7 software using PyCharm Community Edition and Windows 11 Operating System, aiming to enhance the estimation robustness and accuracy under varying wireless channel conditions. In addition, certain other arrangements, including 16 gigabytes of Random Access Memory (RAM), 12 gigabytes of Graphics Processing Unit, and 128 gigabytes of Read Only Memory(ROM), are also maintained to ensure reliable channel estimation. Table 1 summarizes the configuration settings of AseO-CNN's hyperparameters.

Table 1 Configuration settings of AseO-CNN's Hyperparameters

Hyperparameter	Values
Batch size	32
Optimizer	Adam
Dense layer	63,32
Loss function	MSE
1D convolution layer	Filter: 16,32,64 Kernel size: 3,1 Padding: "same"
Batch normalization	Yes
Activation	ReLU
Epochs	500
Pop Size	100

5.2. Performance Metrics

The ASeO-CNN is trained and evaluated under varying signal-to-noise ratio (SNR) conditions on 5G wireless channels. Performance is assessed using Mean Squared Error (MSE), Mean Absolute Error (MAE), Bit Error Rate (BER), Correlation, and R-squared (R^2) metrics. Each of these metrics is described below. BER is the ratio measure of the incorrectly detected bits along the channel. MAE is a measure of the absolute average difference between the actual and the estimated channel coefficients. Meanwhile, the average squared difference between the estimated and the actual channel coefficients defines the MSE. Correlation is the similarity measure between the actual and the estimated channel responses. The ratio measure of the variance in the actual channel models the R-Squared. Together, these metrics provide a comprehensive measure of the ASeO-CNN's channel estimation reliability and accuracy.

5.3. Experimental Results

Figure 5 illustrates the experimental results of the ASeO-CNN proposed for channel estimation. Apparently, the experimental results highlight the varying amplitude of the signal that is transmitted via the original channel and the predicted channel.

5.4. Comparative Methods

The channel estimation performance of the ASeO-CNN is analyzed by varying the SNR values, and its significance is compared with that of the CNN+LSTM [8], SSA-CNN [27], DM-CE [3], 1D-CNN [4], DNN [1], CNN [6], and SSA-CNN [28]. All these methods used for performance assessment are evaluated under the same experimental settings to showcase fairer evaluation.

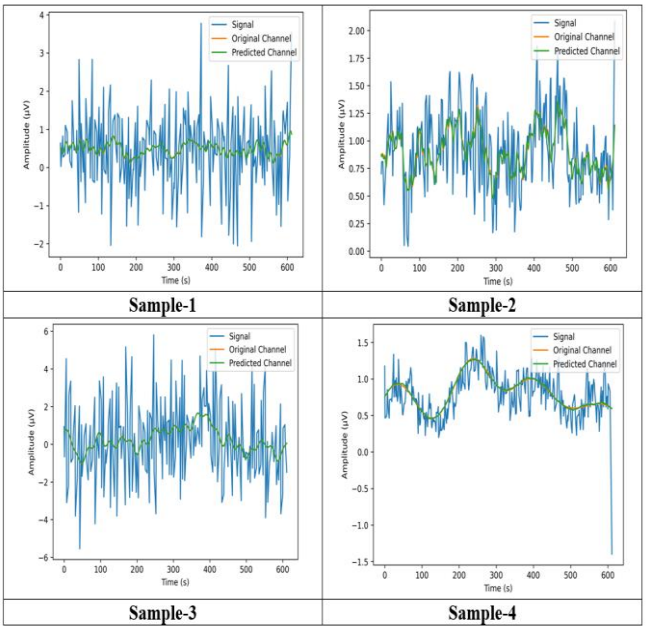

Figure 5: Experimental results of ASeO-CNN

5.4.1. Comparative Analysis with 40 Training Percentages

Figure 6 represents the ASeO-CNN's comparative analysis with 40% training and varying SNR. The ASeO-CNN achieves 0.00014BER with 20dB SNR, surpassing the CNN+LSTM by 0.00032BER, SSA-CNN by 9.29 x 10^{-5} BER, and DM-CE by 0.00025 BER. Eventually, the correlation of 0.913 obtained using the ASeO-CNN exceeds the DNN by 0.024, CNN by 0.022, and SSA-CNN by 0.022. Further, with 0.080 MSE, the ASeO-CNN shows a performance difference of 0.004 with SSA-CNN, 0.042 with DM-CE, and 0.012 with 1D-CNN. In

addition, the ASeO-CNN reveals 0.83 R-square and exceeds the DM-CE, 1D-CNN, and DNN with the relative improvement of 0.12, 0.063, and 0.042, respectively. Moreover, the ASeO-CNN exhibits an MAE of 0.18 and is lower than the CNN+LSTM with 0.24MAE, SSA-CNN with 0.19MAE, and DM-CE by 0.24. From this, the ASeO-CNN demonstrates better channel estimation performance because of the ASeO algorithm that optimally fine-tunes its hyperparameters to promote accurate estimation of the channel coefficients.

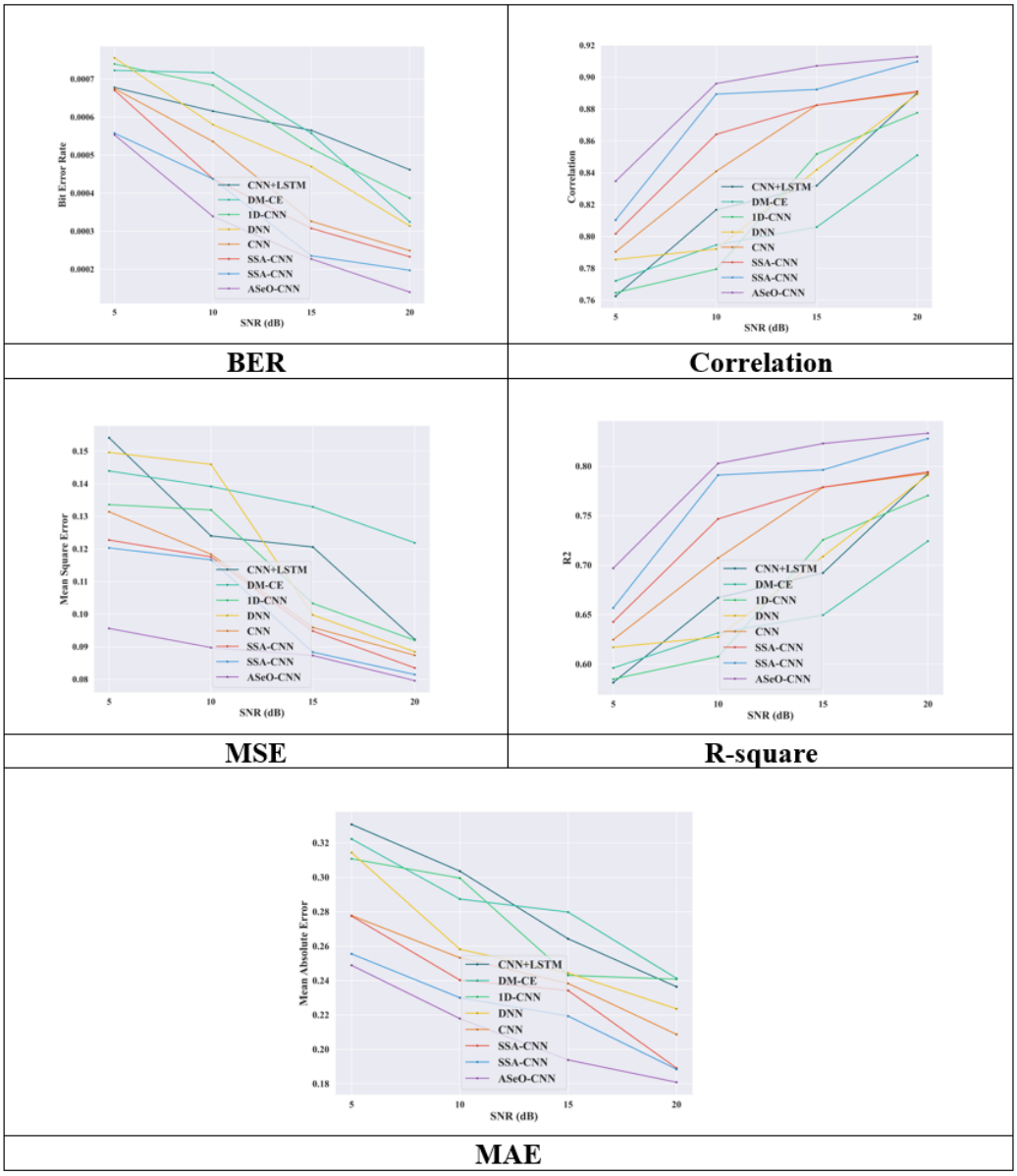

Figure 6 Comparative Analysis of ASeO-CNN with 40 training percentages

5.4.2. Comparative Analysis with 60 training percentages

Figure 7 reveals the ASeO-CNN's comparative analysis with 60% training and varying SNR. Herein, with 20dB SNR, the ASeO-CNN achieves a lower BER of 6.11 x 10-5, while the DM-CE, 1D-CNN, and DNN exhibit higher BER, showing a significant difference of 1.48 x 10-5, 6.50x 10-5, and 8.71 x 10-5, respectively. While the ASeO-CNN shows a higher correlation of 0.953 and outperforms the CNN+LSTM by 0.057, SSA-CNN by 0.003, and DM-CE by 0.034. Furthermore, the MSE of the ASeO-CNN measures 0.0507, while the DNN, CNN, and SSA-CNN reveal 0.02, 0.0037,

and 0.0007 performance differences, respectively. In addition, with the R-Square of 0.909, the AseO-CNN surpasses the CNN+LSTM by 0.12, SSA-CNN by 0.006, and CNN by 0.010. Nevertheless, the MAE of 0.151 attained using the AseO-CNN remains lower than the 0.15 MAE of the SSA-CNN, 0.18 MAE of the DM-CE, and 0.16 MAE of the CNN+LSTM. The spatial feature capturing characteristics of the ASeO-CNN pave the way for accurate channel estimation with reduced computational complexity using its deeper layers.

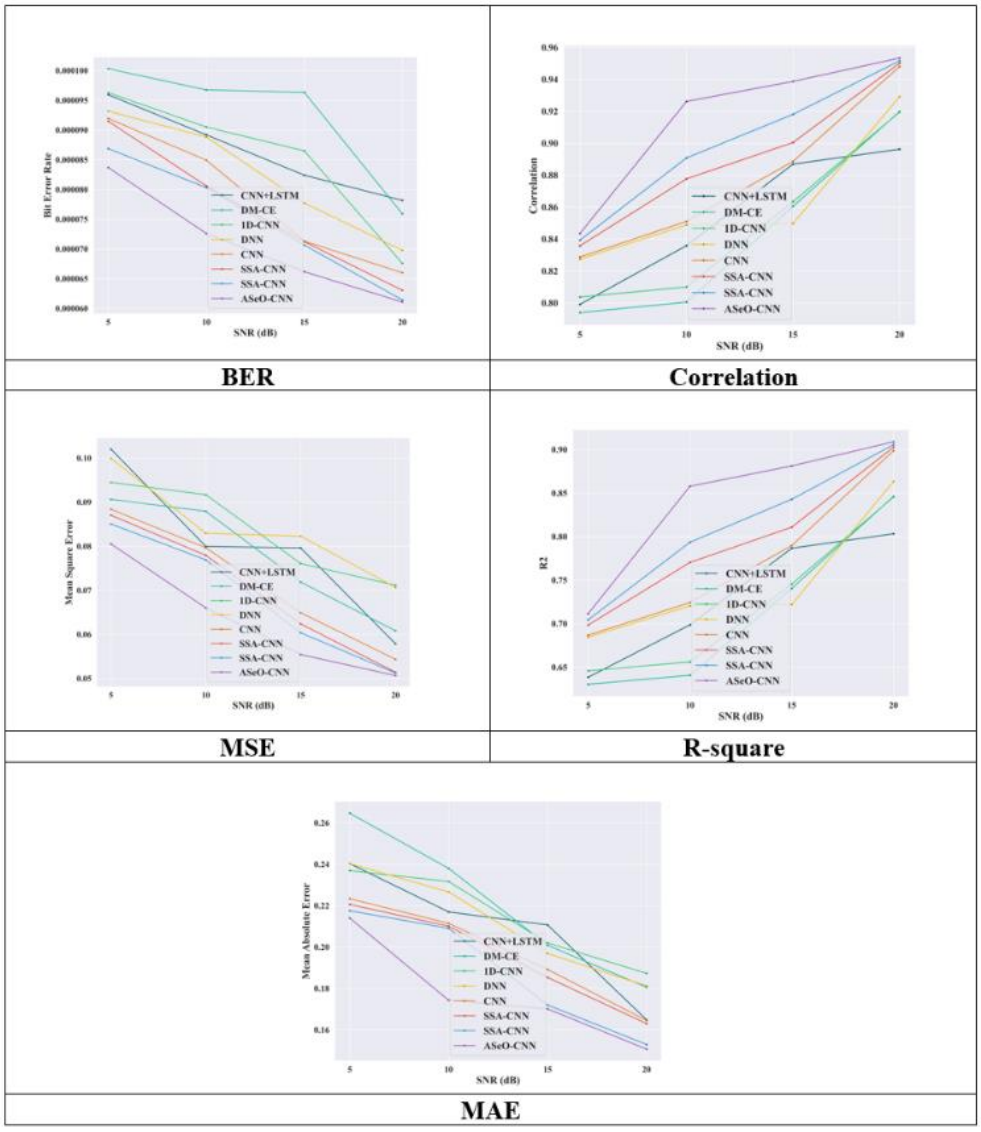

Figure 7 Comparative Analysis of ASeO-CNN with 60 training percentages

5.4.3. Comparative Analysis with 80 training percentages

Figure 8 unveils the comparative analysis of the AseO-CNN with 80% training and varying SNR. The AseO-CNN achieves 5.32 x 10-6 BER with 20dB SNR and shows a performance difference of 1.74 x 10-6 with the CNN+LSTM, 1.28 x 10-6 with the SSA-CNN, and 7.23 x 10-6 with the 1D-CNN. The 0.040MSE of AseO-CNN remains lower than that of the DM-CE by 0.014, CNN by 0.007, and CNN+LSTM by 0.015. Further, the 0.97 correlation obtained using the AseO-CNN surpasses the DNN, CNN, and DM-CE by 0.03, 0.01, and 0.02, respectively. While with an R-Square of 0.933, the AseO-CNN shows improvement over the DNN by 0.06, CNN by 0.02, and SSA-CNN by 0.01. Eventually, the 0.13 MAE of the AseO-CNN is found to be lower than that exhibited using the DM-

CE, 1D-CNN, and DNN, which are 0.16, 0.18, and 0.16, respectively. These achievements signify the advantages of incorporating the pilot signals and performing QAM-based transmission in the AseO-CNN, which promotes both system efficiency and channel estimation quality.

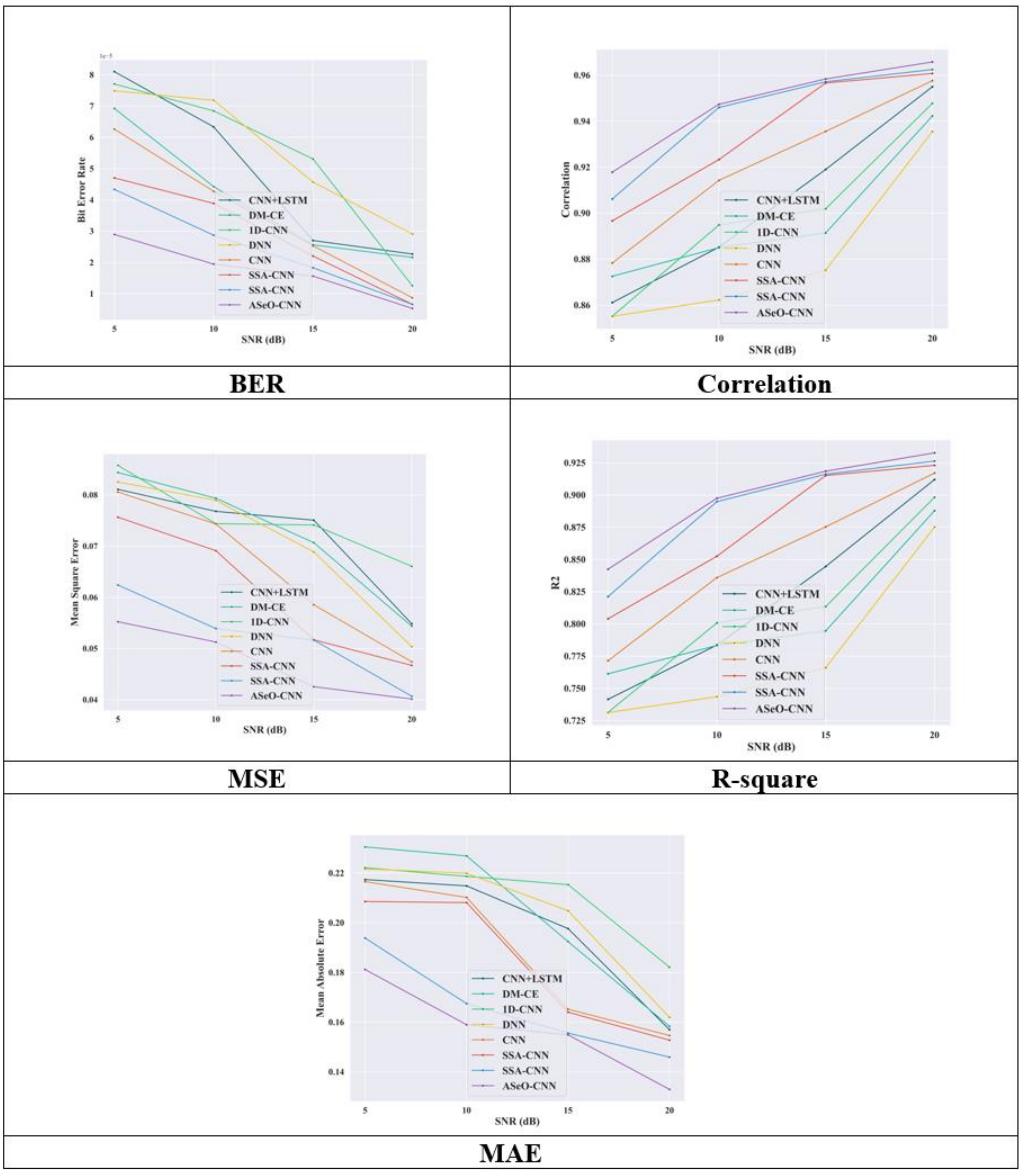

Figure 8 Comparative Analysis of ASeO-CNN with 80 training percentages

5.5. Time complexity analysis

Figure 9 demonstrates the time complexity analysis of the AseO-CNN in channel estimation. The AseO-CNN takes only 188.16s to estimate the channel coefficients in 96 iterations, while the DM-CE, 1D-CNN, DNN, and SSA-CNN take larger times at the order of 196.14s, 196.33s, 196.49s, and 195.61s to perform channel estimation. Hence, the use of the AseO-CNN with its optimized hyperparameters captures complex and nonlinear channel variations and promotes reliable channel estimation.

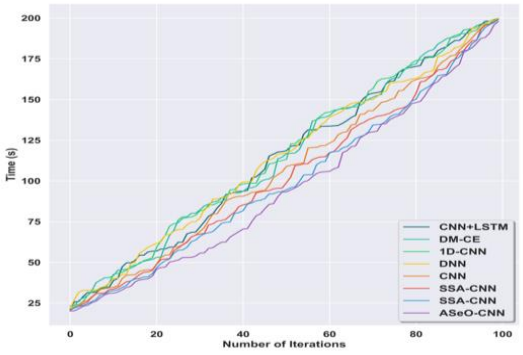

Figure 9 Time complexity Analysis of ASeO-CNN

5.6. Ablation study

The ablation study of the AseO-CNN is revealed in Figure 10. While using only the squirrel search algorithm for the channel estimation, the BER exhibited is found to be higher by about 6.60 x 10-6. At the same time, with the usage of the Sparrow Search Algorithm, the BER is determined to be slightly higher due to the random exploitation characteristics and is given as 6.63 x 10-6. Apparently, the development of the AseO-CNN in channel estimation reduced the BER to 5.32 x 10-6, which influenced reliable wireless communication. These significant improvements are mainly due to the complex spatial feature acquisition characteristics of the AseO-CNN with its optimized hyperparameters.

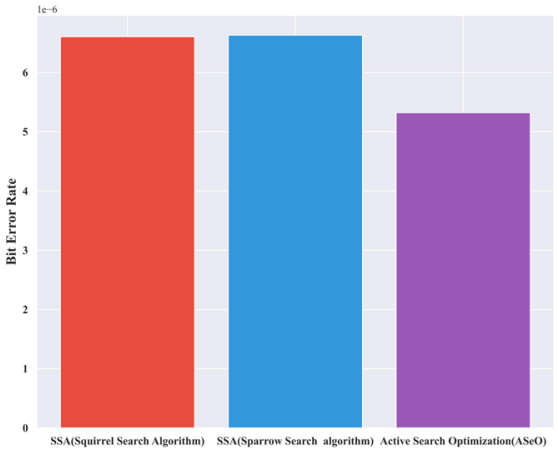

Figure 10 Ablation study of AseO-CNN

5.7. Statistical Analysis

Statistical analysis helps in measuring the ASeO-CNN's robustness in channel estimation under diverse channel conditions. Apparently, certain statistical measures, including the variance, maximum, and mean, are used for characterizing the reliability of the estimated communication channel. Tables 2,3, and 4 provide the statistical analysis of the ASeO-CNN at 40%, 60%, and 90% training.

Table 2 Statistical Analysis of 40% training

Methods/ Metrics		CNN+LSTM	DM-CE	1D-CNN	DNN	CNN	SSA-CNN	SSA-CNN	ASeO-CNN
BER	**Mean**	0.00058	0.00058	0.000582	0.00053	0.000446	0.000412	0.000357	0.000315
	Variance	6.27E-09	2.62E-08	1.93E-08	2.59E-08	2.84E-08	2.76E-08	2.18E-08	2.39E-08
	Maximum	0.000678	0.000723	0.00074	0.000756	0.000675	0.000671	0.000558	0.000553
Correlation	**Mean**	0.83	0.81	0.82	0.83	0.85	0.86	0.88	0.89
	Variance	0.0021	0.0008	0.0023	0.0018	0.0016	0.0012	0.0015	0.0010
	Maximum	0.890	0.851	0.878	0.889	0.890	0.891	0.910	0.913
MAE	**Mean**	0.28	0.28	0.27	0.26	0.24	0.24	0.22	0.21
	Variance	0.0013	0.0008	0.0010	0.0011	0.0006	0.0010	0.0006	0.0007
	Maximum	0.33	0.32	0.31	0.31	0.28	0.28	0.26	0.25
MSE	**Mean**	0.12	0.13	0.12	0.12	0.11	0.10	0.10	0.09
	Variance	0.00048	0.00007	0.00033	0.00074	0.00031	0.00026	0.00029	0.00003
	Maximum	0.15	0.14	0.13	0.15	0.13	0.12	0.12	0.10
R-Square	**Mean**	0.68	0.65	0.67	0.69	0.73	0.74	0.77	0.79
	Variance	0.006	0.002	0.006	0.005	0.004	0.003	0.004	0.003
	Maximum	0.792	0.724	0.770	0.791	0.793	0.794	0.828	0.833

Table 3 Statistical Analysis of 60% training

Methods/ Metrics		CNN+LSTM	DM-CE	1D-CNN	DNN	CNN	SSA-CNN	SSA-CNN	ASeO-CNN
BER	Mean	8.64E-05	9.23E-05	8.52E-05	8.24E-05	7.86E-05	7.66E-05	7.48E-05	7.09E-05
	Variance	4.56E-11	9.23E-11	1.16E-10	8.46E-11	1.08E-10	1.13E-10	9.31E-11	7.14E-11
	Maximum	9.59E-05	0.0001	9.63E-05	9.32E-05	9.20E-05	9.15E-05	8.69E-05	8.37E-05
Correlation	Mean	0.85	0.84	0.85	0.86	0.88	0.89	0.90	0.92
	Variance	0.0016	0.0026	0.0022	0.0015	0.0020	0.0017	0.0017	0.0018
	Maximum	0.8963	0.9199	0.9196	0.9292	0.9481	0.9502	0.9516	0.9534
MAE	Mean	0.21	0.0007	0.24	0.21	0.0007	0.24	0.21	0.0007
	Variance	0.22	0.0011	0.26	0.22	0.0011	0.26	0.22	0.0011
	Maximum	0.21	0.0004	0.24	0.21	0.0004	0.24	0.21	0.0004
MSE	Mean	0.08	0.08	0.08	0.08	0.07	0.07	0.07	0.06
	Variance	0.00024	0.00015	0.00010	0.00011	0.00017	0.00019	0.00018	0.00013
	Maximum	0.10	0.09	0.09	0.10	0.09	0.09	0.09	0.08
R-Square	Mean	0.73	0.71	0.72	0.75	0.77	0.80	0.81	0.84
	Variance	0.004	0.008	0.006	0.005	0.006	0.005	0.005	0.006
	Maximum	0.803	0.846	0.846	0.863	0.899	0.903	0.906	0.909

Table 4 Statistical Analysis of 80% training

Methods/ Metrics		CNN+LSTM	DM-CE	1D-CNN	DNN	CNN	SSA-CNN	SSA-CNN	ASeO-CNN
BER	Mean	4.85E-05	4.02E-05	5.28E-05	5.54E-05	3.49E-05	2.86E-05	2.43E-05	1.74E-05
	Variance	6.01E-10	3.54E-10	6.13E-10	3.59E-10	4.02E-10	2.43E-10	1.83E-10	7.17E-11
	Maximum	8.10E-05	6.92E-05	7.71E-05	7.49E-05	6.26E-05	4.70E-05	4.34E-05	2.90E-05
Correlation	Mean	0.91	0.90	0.90	0.88	0.92	0.93	0.94	0.95
	Variance	0.0013	0.0007	0.0011	0.0010	0.0009	0.0007	0.0005	0.0003
	Maximum	0.95	0.94	0.95	0.94	0.96	0.96	0.96	0.97
MAE	Mean	0.20	0.20	0.21	0.20	0.19	0.18	0.17	0.16
	Variance	0.00058	0.00086	0.00026	0.00058	0.00073	0.00064	0.00032	0.00029
	Maximum	0.22	0.23	0.22	0.22	0.22	0.21	0.19	0.18
MSE	Mean	0.072	0.072	0.075	0.070	0.065	0.061	0.052	0.047
	Variance	0.000102	0.00013	4.92E-05	0.000156	0.00017	0.000143	6.00E-05	3.82E-05
	Maximum	0.081	0.084	0.086	0.083	0.081	0.076	0.062	0.055
R-Square	Mean	0.820	0.807	0.811	0.779	0.850	0.874	0.890	0.898
	Variance	0.004	0.002	0.004	0.003	0.003	0.002	0.002	0.001

	Maximum	0.912	0.888	0.898	0.875	0.917	0.923	0.926	0.933

5.8. T-statistical analysis

T-statistical analysis helps in evaluating whether the observed relationships or the magnitude of differences remain statistically significant in estimating the channel characteristics. The probability(p) value indicates the probability that the predicted improvement occurs by chance. Tables 5, 6, and 7 delineate the t-statistical analysis of the ASeO-CNN.

Table 5 t-statistical Analysis of 40% training

Methods/ Metrics		CNN+LSTM	DM-CE	1D-CNN	DNN	CNN	SSA-CNN	SSA-CNN	ASeO-CNN
BER	T-statistics	2.59	2.74	2.43	2.32	2.03	1.87	1.87	1.96
	p-value	0.08	0.07	0.09	0.10	0.14	0.16	0.16	0.15
Correlation	T-statistics	2.394	2.038	1.959	1.721	2.644	2.881	2.937	2.942
	p-value	0.096	0.134	0.145	0.184	0.077	0.063	0.061	0.060
MAE	T-statistics	2.27	2.49	1.78	1.88	2.48	2.55	2.51	1.97
	p-value	0.11	0.09	0.17	0.16	0.09	0.08	0.09	0.14
MSE	T-statistics	2.41	2.64	2.23	2.07	2.07	2.27	2.06	2.55
	p-value	0.09	0.08	0.11	0.13	0.13	0.11	0.13	0.08
R-Square	T-statistics	2.345	2.007	1.940	1.703	2.622	2.871	2.930	2.938
	p-value	0.1007	0.1384	0.1477	0.1871	0.0788	0.0640	0.0610	0.0606

Table 6 t-Statistical Analysis of 60% training

Methods/ Metrics		CNN+LSTM	DM-CE	1D-CNN	DNN	CNN	SSA-CNN	SSA-CNN	ASeO-CNN
BER	T-statistics	2.12	2.96	2.84	2.37	2.10	2.21	2.40	2.01
	p-value	0.12	0.06	0.07	0.10	0.13	0.11	0.10	0.14
Correlation	T-statistics	2.44	1.69	1.68	1.62	1.93	2.32	2.56	2.92
	p-value	0.09	0.19	0.19	0.20	0.15	0.10	0.08	0.06
MAE	T-statistics	2.74	2.15	2.29	2.22	2.51	2.46	2.29	2.00
	p-value	0.07	0.12	0.11	0.11	0.09	0.09	0.11	0.14
MSE	T-statistics	2.44	2.42	2.12	2.21	2.31	2.30	2.23	1.89
	p-value	0.09	0.09	0.12	0.11	0.10	0.10	0.11	0.16
R-Square	T-statistics	2.41	1.67	1.66	1.59	1.90	2.28	2.53	2.91
	p-value	0.09	0.19	0.19	0.21	0.15	0.11	0.09	0.06

Table 7 t-Statistical Analysis of 80% training

Methods/ Metrics		CNN+LSTM	DM-CE	1D-CNN	DNN	CNN	SSA-CNN	SSA-CNN	ASeO-CNN
BER	T-statistics	1.82	1.71	2.81	2.40	2.26	2.45	2.26	2.46
	p-value	0.17	0.19	0.07	0.10	0.11	0.09	0.11	0.09
Correlation	T-statistics	2.15	1.65	2.36	1.47	2.55	2.50	2.89	2.80
	p-value	0.12	0.20	0.10	0.24	0.08	0.09	0.06	0.07
MAE	T-statistics	2.85	2.58	2.97	2.89	2.05	2.10	1.91	2.43
	p-value	0.07	0.08	0.06	0.06	0.13	0.13	0.15	0.09
MSE	T-statistics	2.93	2.71	2.23	2.75	2.36	2.04	2.57	2.01
	p-value	0.06	0.07	0.11	0.07	0.10	0.13	0.08	0.14
R-Square	T-statistics	2.13	1.63	2.33	1.45	2.53	2.48	2.88	2.79
	p-value	0.12	0.20	0.10	0.24	0.09	0.09	0.06	0.07

5.9. Comparative Discussion

Table 8 shows the comparative discussion of the Aseo-CNN with 20dB SNR under varying training percentages. The Aseo-CNN achieves 5.32 x 10-5 BER, 0.97 correlation, 0.13 Mean Absolute Error, 0.040 Mean Squared Error, and 0.933 R-Squared metrics with 20dB Signal to Noise Ratio in estimating the channel coefficients. These improvements demonstrate the AseO-CNN's significance in eliminating the phase ambiguities faced using the DM-based models[3] via the incorporation of the QAM scheme in data transmission. The introduction of the pilot symbols during data transmission ensured reliable wireless communication by addressing the scalability challenges in using the CNN-CDL[6]. Furthermore, the large number of transmitting and receing antenna present in the AseO-CNN-based framework supported easy handling of a large number of users in the network. Eventually, the AseO-CNN, with its fine-tuned hyperparameters, eliminated the convergence risks in CP-Mamba-based channel estimation models [7] and prevented the AseO-CNN from getting stuck in local optima. Overall, the AseO-CNN offers a reliable solution for fifth-generation wireless communication systems through accurately estimating the CSI with reduced computational complexity and improved adaptability to dynamic environments.

Table 8 Comparative discussion of the AseO-CNN

40% training, SNR-20dB								
Methods/Metrics	CNN+LSTM [8]	DM-CE[3]	1D-CNN [4]	DNN [1]	CNN [6]	SSA-CNN [27]	SSA-CNN [28]	**ASeO-CNN**
BER	0.0005	0.0003	0.0004	0.0003	0.0002	0.0002	0.0002	**0.0001**
Correlation	0.890	0.851	0.878	0.889	0.890	0.891	0.910	**0.913**
MAE	0.24	0.24	0.24	0.22	0.21	0.19	0.19	**0.18**
MSE	0.092	0.122	0.092	0.088	0.087	0.084	0.081	**0.080**
R-square	0.792	0.724	0.770	0.791	0.793	0.794	0.828	**0.833**
60% training, SNR-20dB								
BER	7.82×10^{-5}	7.59×10^{-5}	6.76×10^{-5}	6.98×10^{-5}	6.60×10^{-5}	6.31×10^{-5}	6.14×10^{-5}	**6.11×10^{-5}**
Correlation	0.896	0.920	0.920	0.929	0.948	0.950	0.952	**0.953**
MAE	0.165	0.181	0.187	0.181	0.165	0.163	0.153	**0.151**

MSE	0.0579	0.0608	0.0712	0.0707	0.0543	0.0514	0.0513	**0.0507**
R-square	0.803	0.846	0.846	0.863	0.899	0.903	0.906	**0.909**
80% training, SNR-20dB								
BER	2.27×10^{-5}	2.16×10^{-5}	1.25×10^{-5}	2.91×10^{-5}	8.72×10^{-5}	6.63×10^{-5}	6.60×10^{-5}	**5.32×10^{-5}**
Correlation	0.95	0.94	0.95	0.94	0.96	0.96	0.96	**0.97**
MAE	0.16	0.16	0.18	0.16	0.15	0.15	0.15	**0.13**
MSE	0.055	0.054	0.066	0.050	0.047	0.047	0.041	**0.040**
R-square	0.912	0.888	0.898	0.875	0.917	0.923	0.926	**0.933**

Conclusion

The research presented an ASeO-CNN model for accurate wireless channel estimation. The ASeO algorithm integrated within the ASeO-CNN enables accurate learning of the complex channel characteristics to promote optimal channel estimation. Moreover, the ability of the ASeO-CNN to capture the non-linear channel characteristics enhanced the communication reliability and channel estimation. Furthermore, the pilot signal utilization improves synchronization and reduces the estimation uncertainties by providing reliable reference details for accurate channel estimation even in dynamic and noisy environments. In essence, the QAM adopted promotes better spectral efficiency through enabling reliable transmission of more bits per symbol. Thereby, achieving better data throughput with effective communication performance maintenance. The results indicate that ASeO-CNN achieves better channel performance in terms of 5.32×10^{-5} BER, 0.97 correlation, 0.13 Mean Absolute Error, 0.040 Mean Squared Error, and 0.933 R-Squared metrics with 20dB Signal to Noise Ratio. Future work will focus on expanding the ASeO-CNN to real-time deployment scenarios and massive MIMO, millimetre wave communications through integrating with Reconfigurable Intelligent Surface(RIS) systems.

References

[1]. Hashempoor, H. and Choi, W., 2025. Deep learning-based data-assisted channel estimation and detection. IEEE Transactions on Machine Learning in Communications and Networking.

[2]. Nazim, M.S., Nguyen, H., and Jang, Y.M., 2025. Channel estimation of massive MIMO FSO communication system using deep attention residual U-Net. ICT Express, 11(2), pp.287-292.

[3]. Zhou, X., Liang, L., Zhang, J., Jiang, P., Li, Y., and Jin, S., 2025. Generative diffusion models for high-dimensional channel estimation. IEEE Transactions on Wireless Communications.

[4]. Siriwanitpong, A., Sanada, K., Hatano, H., Mori, K., and Boonsrimuang, P., 2025. Deep learning-based channel estimation with 1D CNN for OFDM systems under high-speed railway environments. IEEE Access, 13, pp.13128-13142.

[5]. Gao, Y., Chen, Q., He, L., Wang, Z., Huang, Y., Zhang, J., Gao, Y. and Xu, Z., 2026. Artificial intelligence enabled joint channel estimation and signal detection for massive MIMO systems. Chinese Journal of Electronics, 35(1), pp.178-195.

[6]. Zheng, P., Lyu, X., Wang, Y. and Gong, Y., 2025. Convolutional dictionary learning-based hybrid-field channel estimation for XL-RIS-aided massive MIMO systems. IEEE Transactions on Wireless Communications.

[7]. Li, Z., Zheng, C., Xiao, J., Wang, J., Wang, G., Zeng, M., and Dobre, O.A., 2026. Deep Learning Based Joint Channel Estimation and Positioning for Sparse XL-MIMO OFDM Systems. IEEE Transactions on Vehicular Technology.

[8]. Tian, X. and Zheng, Q., 2025. A massive MIMO channel Estimation method based on a hybrid deep learning model with regularization techniques. International Journal of Intelligent Systems, 2025(1), p.2597866.

[9]. Soltani, M., Pourahmadi, V., Mirzaei, A. and Sheikhzadeh, H., 2019. Deep learning-based channel estimation. IEEE Communications Letters, 23(4), pp.652-655.

[10]. Amirabadi, M.A., Kahaei, M.H.,

Nezamalhosseini, S.A. and Vakili, V.T., 2020. Deep learning for channel estimation in FSO communication systems. Optics Communications, 459, p.124989.

[11]. He, H., Wen, C.K., Jin, S., and Li, G.Y., 2018. Deep learning-based channel estimation for beamspace mmWave massive MIMO systems. IEEE Wireless Communications Letters, 7(5), pp.852-855.

[12]. Kang, J.M., Chun, C.J., and Kim, I.M., 2020. Deep learning-based channel estimation for MIMO systems with received SNR feedback. IEEE Access, 8, pp.121162-121181.

[13]. Wei, L., Huang, C., Alexandropoulos, G.C., Yuen, C., Zhang, Z. and Debbah, M., 2021. Channel estimation for RIS-empowered multi-user MISO wireless communications. IEEE Transactions on Communications, 69(6), pp.4144-4157.

[14]. Han, Y., Jin, S., Wen, C.K. and Ma, X., 2020. Channel estimation for extremely large-scale massive MIMO systems. IEEE Wireless Communications Letters, 9(5), pp.633-637.

[15]. Wang, Z., Liu, L., and Cui, S., 2020, May. Channel estimation for intelligent reflecting surface-assisted multiuser communications. In 2020, IEEE Wireless Communications and Networking Conference (WCNC) (pp. 1-6). IEEE.

[16]. Bai, Q., Wang, J., Zhang, Y., and Song, J., 2019. Deep learning-based channel estimation algorithm over time-selective fading channels. IEEE Transactions on Cognitive Communications and Networking, 6(1), pp.125-134.

[17]. Balevi, E., Doshi, A. and Andrews, J.G., 2020. Massive MIMO channel estimation with an untrained deep neural network. IEEE Transactions on Wireless Communications, 19(3), pp.2079-2090.

[18]. Ma, S., Wang, G., Fan, R. and Tellambura, C., 2018. Blind channel estimation for ambient backscatter communication systems. IEEE Communications Letters, 22(6), pp.1296-1299.

[19]. Dovelos, K., Matthaiou, M., Ngo, H.Q. and Bellalta, B., 2021. Channel estimation and hybrid combining for wideband terahertz massive MIMO systems. IEEE Journal on Selected Areas in Communications, 39(6), pp.1604-1620.

[20]. Mashhadi, M.B. and Gündüz, D., 2021. Pruning the pilots: Deep learning-based pilot design and channel estimation for MIMO-OFDM systems. IEEE Transactions on Wireless Communications, 20(10), pp.6315-6328.

[21]. Le, H.A., Van Chien, T., Nguyen, T.H., Choo, H., and Nguyen, V.D., 2021. Machine learning-based 5G-and-beyond channel estimation for MIMO-OFDM communication systems. Sensors, 21(14), p.4861.

[22]. Yi, X. and Zhong, C., 2020. Deep learning for joint channel estimation and signal detection in OFDM systems. IEEE Communications Letters, 24(12), pp.2780-2784.

[23]. Yang, Y., Gao, F., Ma, X., and Zhang, S., 2019. Deep learning-based channel estimation for doubly selective fading channels. IEEE Access, 7, pp.36579-36589.

[24]. Liu, X., Zeng, X., Liu, C., Liu, W., and Zhang, Y., 2017. The channel estimation and modeling in a high altitude platform station wireless communication dynamic network. Discrete Dynamics in Nature and Society, 2017(1), p.5939810.

[25]. Ma, X. and Gao, Z., 2020. Data-driven deep learning to design a pilot and channel estimator for massive MIMO. IEEE Transactions on Vehicular Technology, 69(5), pp.5677-5682.

[26]. Elbir, A.M. and Coleri, S., 2021. Federated learning for channel estimation in conventional and RIS-assisted massive MIMO. IEEE transactions on wireless communications, 21(6), pp.4255-4268.

[27]. Zheng, T. and Luo, W., 2019. An improved squirrel search algorithm for optimization. Complexity, 2019(1), p.6291968.

[28]. Xue, J. and Shen, B., 2020. A novel swarm intelligence optimization approach: Sparrow Search Algorithm. Systems science & control engineering, 8(1), pp.22-34.

[29]. Ye, H., Li, G.Y. and Juang, B.H., 2017. Power of deep learning for channel estimation and signal detection in OFDM systems. IEEE Wireless Communications

Letters, 7(1), pp.114-117.
[30]. Khan, I., Cheffena, M. and Hasan, M.M., 2023. Data-aided channel estimation for MIMO-OFDM wireless systems using reliable carriers. IEEE Access, 11, pp.47836-47847.
[31]. Jebur, B.A., Alkassar, S.H., Abdullah, M.A., and Tsimenidis, C.C., 2021. Efficient machine learning-enhanced channel estimation for OFDM systems. IEEE Access, 9, pp.100839-100850.
[32]. Mohammed, A.S.M., Taman, A.I.A., Hassan, A.M., and Zekry, A., 2023. Deep learning channel estimation for OFDM 5G systems with different channel models. Wireless Personal Communications, 128(4), pp.2891-2912.
[33]. Wang, M., Wang, A., Liu, Z., and Chai, J., 2023. Deep learning-based channel estimation method for mine OFDM system. Scientific Reports, 13(1), p.17105.
[34]. Ali, M.H.E., Rabeh, M.L., Hekal, S., and Abbas, A.N., 2022. Deep learning gated recurrent neural network-based channel state estimator for OFDM wireless communication systems. IEEE Access, 10, pp.69312-69322.
[35]. Wang, B., Jian, M., Gao, F., Li, G.Y. and Lin, H., 2019. Beam squint and channel estimation for wideband mmWave massive MIMO-OFDM systems. IEEE transactions on signal processing, 67(23), pp.5893-5908.